Cochlea's Graded Curvature Effect on Low Frequency Waves

D. Manoussaki,[1] E. K. Dimitriadis,[2] and R. S. Chadwick[3]

[1]*Department of Mathematics, Vanderbilt University, Nashville, Tennessee 37240, USA*
[2]*Division of Bioengineering & Physical Science, ORS/OD, National Institutes of Health, Bethesda, Maryland 20892, USA*
[3]*Section on Auditory Mechanics, NIDCD, National Institutes of Health, Bethesda, Maryland 20892, USA*

(Received 22 June 2005; published 2 March 2006)

In the ear, sound waves are processed by a membrane of graded mechanical properties that resides in the fluid-filled spiral cochlea. The role of stiffness grading as a Fourier analyzer is well known, but the role of the curvature has remained elusive. Here, we report that increasing curvature redistributes wave energy density towards the cochlea's outer wall, affecting the shape of waves propagating on the membrane, particularly in the region where low frequency sounds are processed.

DOI: 10.1103/PhysRevLett.96.088701 PACS numbers: 43.64.+r, 42.15.Dp, 46.40.Cd, 47.35.−i

In the ear, sound processing takes place on the cochlea's basilar membrane (BM). Sounds are transmitted to the cochlear fluids, which interact mechanically with the membrane, causing it to vibrate in the form of a traveling wave that propagates along the membrane's length (Fig. 1). Because of the BM's graded stiffness, wave amplitude changes as the wave propagates and is maximized at a membrane stiffness characteristic to a certain frequency. The BM thus decomposes incoming sounds into their component frequencies, and is often characterized as a Fourier analyzer designed by nature. Other anatomical features of the cochlea have also been shown to affect the physics of hearing: the maximized BM amplitude interacts with the cochlear microstructure to generate radial shearing forces that open ion channels in neurosensory hair cells. But the role of perhaps the most characteristic feature of the cochlea, its graded curvature forming a spiral shell, has remained elusive.

The long-standing impression is that the spiral shape does not affect hearing, and that the shape facilitates packing the cochlea into a small space. Physical and mathematical models have shown that curvature does not affect maximum amplitude of the BM's centerline [1–3], nor shift the maximum amplitude place along the BM [4]. Mammalian behavioral audiograms, however, suggest otherwise. Statistics point at a strong correlation between number of spiral turns and low frequency hearing thresholds [5]. The question arises whether, in studying the effect of curvature, the appropriate physical quantities were examined. Wave energy remains constant as BM waves travel along the cochlear duct, because the change of cochlear dimensions, including curvature, are very slow [6]. Since wave energy is conserved, one could argue that quantities that are averaged over the duct cross-section are also conserved. Wave amplitude at the BM midline may not be affected by curvature, since the midline could be thought of as being close to a cross-sectional average. Curvature, however, has been shown to generate a radial gradient in the fluid pressure [3]. Given that neurosensory cells are stimulated by radial shear forces, it is surprising that radial shear or radial changes in the BM wave amplitude have not been examined in curved models and the mechanics of wave transmission have been studied on straight models instead.

In this Letter, we report that cochlear curvature, by redistributing wave energy density across the duct width, enhances radial shearing in the BM region where low frequency sounds are analyzed. We explain energy redistribution by drawing an analogy between wave energy flow and geometric optics. In explaining the ''whispering gallery'' phenomenon in London's St. Paul cathedral, Rayleigh [7] showed that a pencil of rays emanating from a source towards a nearby concave boundary would, after any number of reflections, be confined near the boundary. In the cochlea, rays represent wave energy propagation paths reflecting off the concave outer wall. We find, however, that the curvature gradient has an additional role: by reflecting off a wall of decreasing radius of curvature, rays progressively focus on the outer wall, corresponding to an increase in wave energy density. The effect is strongest at the cochlear spiral end (apex), which has the smallest radius of curvature and where low frequency sounds are analyzed. This suggests an effect of the cochlear spiral on low frequency sound perception.

To isolate and quantify the effect of curvature on the BM traveling wave, we ignore all geometrical factors other than curvature and BM mass and stiffness. Our simplification extends to considering a BM of constant width (equal to duct width). The fluid is assumed incompressible, irrotational (with velocity $\mathbf{v} = \nabla\Phi$), contained in two ducts symmetrically divided by the BM. If the upper and lower domains are symmetric, it suffices to look at the mass conservation and the (spatially integrated) linearized momentum equations of the lower duct [8]:

$$\nabla^2\Phi = 0, \tag{1}$$

$$P_2 + \rho\frac{\partial\Phi}{\partial t} = 0. \tag{2}$$

Moreover, if the fluid pressure right above and below the

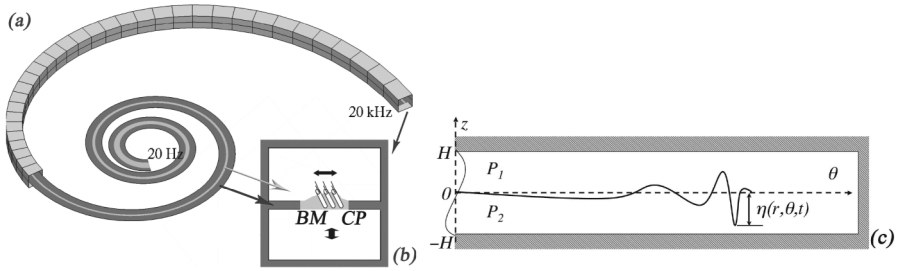

FIG. 1. (a) The cochlea is modeled as a fluid-filled spiral domain, separated by the cochlear partition (CP) into upper and lower fluid ducts. A blowup of the spiral model cross section is shown in (b). Part of the CP is the elastic basilar membrane (light gray), which is designed to respond to high frequencies (20 kHz for humans) at the base and progressively to lower frequencies towards the apex, where the BM is widest and most compliant and responds to about 20 Hz. (c) Side view of the wavelike displacement of the BM in a rolled out cochlea. Incoming sounds, transmitted to the cochlear fluids via a membrane covering the entry of the duct (between $z = 0$ and $z = H$), initiate a traveling wave on the BM. Wave amplitude (normally up to a few nanometers) has been exaggerated to illustrate the wave (*drawn after* [8].)

interface are P_1 and P_2, symmetry implies $P_1 = -P_2$ and the continuity and interface equations become

$$\frac{\partial \eta}{\partial t} = \frac{\partial \Phi}{\partial z}, \tag{3}$$

$$m\frac{\partial^2 \eta}{\partial t^2} + \beta\frac{\partial \eta}{\partial t} + \kappa\eta = P_2 - P_1 = 2P_2, \tag{4}$$

where η is the BM displacement normal to the interface. Equation (4) assumes that the BM and associated cells have been flattened to an interface that has mass m, damping β, and stiffness κ (which can change along the spiral) and that there is no appreciable axial elastic coupling between adjacent regions [9].

We examine the equations in a spiral orthogonal coordinate system (r, θ, z). The distance between a fixed origin and the spiral duct midline is described by a curve $R_m(\theta)$ that slowly decreases with traversed angle θ, while r and z are the horizontal and vertical distance, both measured from the duct midline $R_m(\theta)$ and normal to it. The velocity potential is written in terms of an axial wave number K and input frequency ω, as

$$\Phi(r, \theta, z, t) = \Phi_0(r, \theta, z)e^{i[\omega t - \int_0^\theta K(\theta)R_m(\theta)d\theta]}, \tag{5}$$

where Φ_0 is a slowly varying function of the angular coordinate θ. The axial, transverse, and radial velocities are given in terms of this potential, respectively, as

$$V_\theta = \frac{1}{R_m + r}\frac{\partial \Phi}{\partial \theta} \cong -\frac{iKR_m}{R_m + r}\Phi, \qquad V_z = \frac{\partial \Phi}{\partial z}, \qquad V_r = \frac{\partial \Phi}{\partial r}. \tag{6}$$

The solution to Laplace's equation for the potential Φ, subject to the no-flux condition through the duct bottom located at $z = -H$, allows Φ_0 to take the separated form

$$\Phi_0(\theta, r, z) = A(\theta)C[\mu(r + R_m)]\cosh[\mu(z + H)] \tag{7}$$

where C is a cylinder function satisfying

$$\left(R^2\frac{d^2}{dr^2} + R\frac{d}{dr} + \mu^2R^2 - K^2R_m^2\right)C(\mu R) = 0, \tag{8}$$

$R = r + R_m$, and μ is the separation constant. In the frequency domain, the momentum, continuity, and interface conditions (2)–(4) become

$$P_2 = -i\rho\omega\Phi, \tag{9}$$

$$i\omega\eta = \frac{\partial \Phi}{\partial z} = \mu A(\theta)C[\mu(r + R_m)]\sinh(\mu H), \tag{10}$$

$$2P_2 = (\kappa - m\omega^2 + i\omega\beta)\eta. \tag{11}$$

From the above equations we get the intermediate relation

$$\mu H\tanh(\mu H) = \frac{2H\rho\omega^2}{\kappa - m\omega^2 + i\omega\beta} \tag{12}$$

which, together with (19), will form the dispersion relation. Simple solutions of μ can be obtained for low enough frequencies. Assuming negligible CP damping ($\beta = 0$), and for small values of the parameter μH (set $\mu H = \epsilon \ll 1$) Eq. (12) is written as

$$\mu^2H^2 \approx \frac{2H\rho\omega^2}{\kappa - m\omega^2} \ll 1. \tag{13}$$

The above inequality may be rewritten as $\omega^2 \ll \frac{\kappa}{2\rho H + m}$ which gives the low frequency upper bound. Clearly, this bound is the square of the natural frequency of the local BM oscillator which has a local stiffness of κ and mass equal to the BM mass m, plus the mass of the underlying and overlying fluid, $2\rho H$ per unit length. This is a critical parameter in cochlear mechanics since any given frequency propagates only up to, and has a maximum amplitude near, the axial location with the same natural frequency. Therefore, the low frequency solutions of the dispersion relation are relevant for all frequencies that propagate to the apical end of the duct.

At low frequencies, the cylinder function $C(\mu R)$ can be found by expanding Eq. (8) for small values of ϵ and satisfying the no-flux boundary conditions $C_r = 0$ at the side walls, located at distance r_w from the center line (side walls at $R = R_m - r_w$ and $R = R_m + r_w$). For $\epsilon = \mu H$ and $\zeta = \frac{R}{H}$ we set

$$C(\mu R) = C(\epsilon\zeta) = F_0(\zeta) + \epsilon^2 F_1(\zeta) + \cdots, \tag{14}$$

$$KR_m = k_0 + \epsilon k_1 + \cdots, \tag{15}$$

and find that, to $O(1)$ $F_0 = 1$ and $k_0 = 0$, while, for higher order

$$F_1 = -\tfrac{1}{4}\zeta^2 + \tfrac{1}{2}k_1^2(\log\zeta)^2 + B\log\zeta, \tag{16}$$

$$k_1^2 = \frac{\zeta_2^2 - \zeta_1^2}{2\log(\zeta_2/\zeta_1)} \tag{17}$$

where

$$B = \frac{\zeta_1^2\log\zeta_2 - \zeta_2^2\log\zeta_1}{2\log(\zeta_2/\zeta_1)}, \tag{18}$$

$\zeta_1 = (R_m - r_w)/H$ and $\zeta_2 = (R_m + r_w)/H$. Note that the first term of the expansion of $\log(\zeta_1/\zeta_2)$ for small r_w/R_m is $\log(R_m + r_w/R_m - r_w) \approx 2r_w/R_m$. This, in turn, gives $k_1 \approx R_m/H$, and therefore

$$K \approx \mu; \tag{19}$$

i.e., the wavenumber is unaffected by curvature.

The wave amplitude $A(\theta)$ of the potential function is computed from energy flow conservation along the duct which considers pressure $\times$ horizontal velocity amplitude, calculated over the duct cross section, is constant:

$$\int_{-r_w}^{r_w}\int_{-H}^{0} |P||V_\theta| dz dr = \text{const} \tag{20}$$

Substituting pressure and velocity from (9) and (6) the energy conservation law becomes

$$KR_m \int_{-r_w}^{r_w}\int_{-H}^{0} \left\{\frac{\Phi_0^2}{r + R_m}\right\} dz dr = \text{const} \tag{21}$$

We substitute Φ_0 from (7), into Eq. (21) and assume that for small μH, $\cosh[\mu(\zeta + H)] \approx 1$, so that we get

$$KR_m A(\theta)^2 H \int_{-r_w}^{r_w} \frac{C^2[\mu(r + R_m)]}{r + R_m} dr = \text{const.} \tag{22}$$

We evaluate the above by approximating $C[\mu(r + R_m)] \approx F_0 = 1$, and for small μH assuming $\sinh(\mu H) \approx \mu H$. Assuming further that r_w/R_m is small and using (10) and (19) we solve for the wave amplitude η:

$$\eta(r, \theta) = \gamma\mu^{3/2}H^{1/2}r_w^{-1/2}C[\mu(r + R_m)] \tag{23}$$

where γ is a constant. We set $\alpha = \gamma\mu^{3/2}(H/r_w)^{1/2}$ and calculate, for small r_w/R_m and $r_w \approx H$:

$$\frac{\eta^{\text{out}} - \eta^{\text{in}}}{2r_w} = \frac{\alpha}{2r_w}\{C[\mu(R_m + r_w)] - C[\mu(R_m - r_w)]\} \approx \gamma\frac{\mu^{7/2}r_w^2}{2}\frac{1}{R_m} \tag{24}$$

Equation (24) indicates that the BM-fluid interface gets tilted across the width of the partition, and the radial amplitude slope varies as $1/R_m$. The $1/R_m$ dependence carries over when comparing the amplitude difference between outside and inside walls, to the amplitude η^{str} of a wave propagating in a straight duct

$$\frac{\eta^{\text{out}} - \eta^{\text{in}}}{\eta^{\text{str}}} = \mu^2 r_w^3 \frac{1}{R_m}. \tag{25}$$

As the wave propagates along the BM, its wavelength λ becomes shorter, and thus $\mu \approx K = 2\pi/\lambda$ increases. Therefore, Eqs. (24) and (25) show that increased values of μ towards the apex further increase the radial amplitude tilt. This tilt can also be thought of as contributing a dynamic rotation to the BM, which displaces radially the sensory hair cells' upper surface, located at a distance L above the BM, by

$$L\frac{\Delta\eta/(2r_w)}{\eta} \approx \frac{\mu^2 r_w^2}{2}\frac{L}{R_m} \approx \frac{2\pi^2 r_w^2}{\lambda^2}\frac{L}{R_m} \tag{26}$$

also varying as $1/R_m$. As an example, in the human ear, a frequency of 200 Hz has a wavelength $\lambda \approx 4$ mm [4], hair cell-BM distance $L = 0.15$ mm, $r_w = 0.5$ mm and, assuming that at the apex $R_m \approx r_w$, the radial displacement per unit of BM displacement is about 0.2. This is comparable to measurements at the apex by Fridberger *et al.* [10]. The computed value may, in fact, be larger for the more realistic anatomy of a (radially) increasing L. Since the surface spanning the hair cell tops (reticular lamina) is, at rest, at an angle to the BM, the rotational kinematics of the BM movement could further enhance the radial displacement of the reticular lamina.

Another anatomical simplification in the model was that of a BM width equal to the duct width. A realistic apical BM position and width within the duct was considered in Refs. [3,11] who report a significant apical radial pressure gradient at R_m. While those models cannot predict a BM tilt, they can predict the radial pressure gradient at R_m, which is proportional to BM tilt in the present model. Calculations show that the gradient, as calculated in Ref. [11] is about 25% less than that of the current model.

Our findings are also consistent with our finite element model of cochlear micromechanics [12]. That model includes the anatomically realistic cross-sectional microstructure and shows that curvature greatly improves shear gain, a measure of hair bundle shearing sensitivity, at the BM's low frequency region. How accurate is the effect we are reporting? While the asymptotic analysis was carried out assuming a small ϵ, the ϵ we use, i.e., $\mu H \approx \frac{2\pi}{\lambda}H$ is

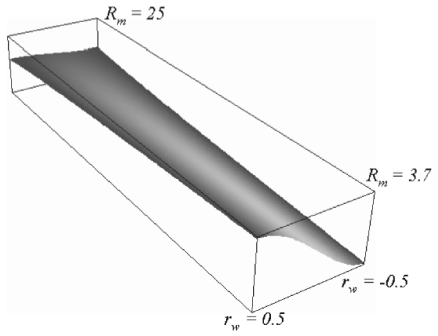

FIG. 2. Wave amplitude, computed from the energy conservation law (22) gets progressively tilted as the wave travels from the cochlear base (midline assumed at radial distance $R_m = 25$) to the cochlear apex ($R_m = 3.7$). The wave amplitude along the spiral length is shown in a straight box, rather than the coiled duct, to show the effect more clearly. r_w is the distance of the sidewall from R_m. The amplitude increases on the outside ($r_w = 0.5$) wall and decreases on the inside ($r_w = -0.5$) wall in the propagation direction.

not so small, and for a wavelength $\lambda \approx 4$ mm and $H = 0.5$ mm, $\epsilon^2 \approx 0.6$. However, when we computed the wave number [from Eq. (12)] and amplitude numerically we found it to be in good agreement to our analytical approximation. In particular, the computations show that our main result, that wave amplitude tilt varies as $1/R_m$, holds for such larger values of ϵ, and the computed tilt is shown in Fig. 2. Our computations also indicate that the restriction $\omega^2 \ll \frac{\kappa}{2\rho H + m}$, can be relaxed for larger values of ω.

What is then a simple, intuitive explanation of the radial wave amplitude tilt? One might attribute it to the quadratic centripetal acceleration term, but this is neglected in our linear analysis. We explain energy density redistribution by drawing an analogy between wave energy density and the density of a pencil of rays propagating along a spiral duct. Ray redistribution would correspond to energy density redistribution which, in turn, would affect the wave amplitude tilt. In a constant radius of curvature duct, rays maintain their distribution near the outer wall, as in St. Paul's whispering gallery. In the spiral duct, the decreasing radius of curvature continuously concentrates the rays near the outer boundary, and thus the equivalent wave energy density gets continuously redistributed towards the outside wall as the wave spirals inwards. The effect is clearly seen in Fig. 3. Rays focus near the outside wall because curvature increases slowly. By doing so, two things are achieved: (i) after a number of reflections, a ray will eventually reflect only off the outer wall, and (ii) as a ray propagates inwards, the angle subtending two subsequent reflection points will stay approximately constant. A cord of a larger circle will be further away from its corresponding arc than a cord that is subtended by an equal angle but on a smaller circle; i.e., smaller radii of curvature force rays to ''get closer'' to the outer wall, where ray density becomes greater.

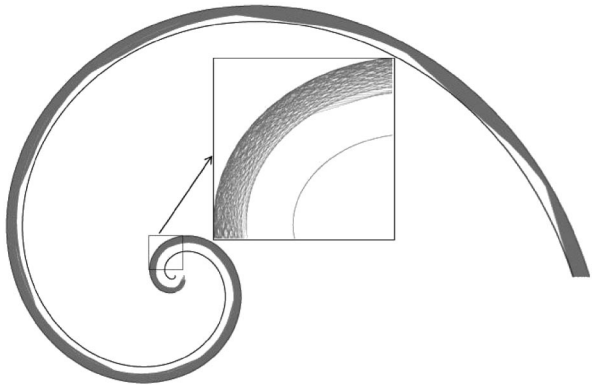

FIG. 3. A stream of rays spanning the channel entry progressively focuses on the outer boundary as they travel inwards along the spiral. Inset shows rays focusing on the outer $1/3$ of the duct's width.

The analysis of our present model allows for quantification of the amplification. If μ and r_w do not vary significantly along the spiral, we calculate that the ratio of the wave tilt at the apex to tilt at the base is

$$\frac{\Delta\eta_{\text{apex}}}{\Delta\eta_{\text{base}}} \approx \frac{R_{m_{\text{base}}}}{R_{m_{\text{apex}}}}. \tag{27}$$

A decrease in radius from the outside of the spiral to the inside by a factor of 10 would then represent a 20 dB amplification due to curvature alone.

We would like to thank S. T. Pantelides and L. Tsetseris for very helpful comments and discussions, and the NIH intramural program and Vanderbilt University, where part of this work was carried out.

[1] M. A. Viergever, J. Acoust. Soc. Am. **64**, 1048 (1978).
[2] C. H. Loh, J. Acoust. Soc. Am. **74**, 95 (1983).
[3] C. R. Steele and J. G. Zais, J. Acoust. Soc. Am. **77**, 1849 (1985).
[4] G. von Békésy, *Experiments in Hearing* (McGraw-Hill, New York, 1960).
[5] C. D. West, J. Acoust. Soc. Am. **77**, 1091 (1985).
[6] M. J. Lighthill, *Waves in Fluids* (Cambridge University Press, Cambridge, England, 1979).
[7] L. Rayleigh, *The Theory of Sound* (Dover Publications, New York, 1945), Vol. II.
[8] M. B. Lesser and D. A. Berkley, J. Fluid Mech. **51**, 497 (1972).
[9] E. deBoer, in *The Cochlea*, edited by P. Dallos *et al.* (Springer Verlag, New York, 1996).
[10] A. Fridberger and J. B. de Monvel, Nat. Neurosci. **6**, 446 (2003).
[11] D. Manoussaki and R. S. Chadwick, SIAM J. Appl. Math. **61**, 369 (2000).
[12] H. Cai, D. Manoussaki, and R. S. Chadwick, J. R. Soc. Interface **2**, 341 (2005).